Computer Modeling in
Engineering & Sciences

Tech Science Press

https://doi.org/10.32604/cmes.2026.081429

ARTICLE

Quantum-Enhanced Transparent Contour-Integral Deep Learning for Fair and Explainable Medical Biometric Authentication

Karthick Raghunath K. M.[1], **Manjula V.**[1], **Mahesh T. R.**[1], **Surbhi B. Khan**[2,3,*], **Ahmed Alyahya**[4,*] and **Shakila Basheer**[5]

[1]Department of Computer Science and Engineering, JAIN (Deemed-to-be University), Bangalore, India
[2]School of Science, Engineering and Environment, University of Salford, Salford, UK
[3]Centre for Research Impact & Outcome, Chitkara University Institute of Engineering and Technology, Chitkara University, Rajpura, Punjab, India
[4]Department of Information Systems, College of Computer Science and Information Technology, King Faisal University, Al-Ahsa, Saudi Arabia
[5]Department of Information Systems, College of Computer and Information Science, Princess Nourah bint Abdulrahman University, P.O. Box 84428, Riyadh, 11671, Saudi Arabia

*Corresponding Authors: Surbhi B. Khan. Email: s.khan138@salford.ac.uk, surbhibhatia1988@yahoo.com; Ahmed Alyahya. Email: aaalyahya@kfu.edu.sa

Received: 02 March 2026; Accepted: 30 April 2026; Published: 27 July 2026

ABSTRACT: In general, medical biometric datasets, with the essential unique behavioral and physical traits for personalized healthcare, shape the patient identification process, but the tendency towards transparency and fairness is still far away. Most of the existing methods fail to integrate the latest mathematical techniques rigorously with the deep learning models, which eventually makes such models undesirable due to their lack of interpretability and potential bias. As such, in this study, a novel Contour Integrated Transparent Augmented Deep Learning (CITADL) methodology is introduced to bridge this gap. In this study, a structured framework, namely CITADL, combines contour-based mathematical feature transformation with a deep neural network architecture empowered with eXplainable Artificial Intelligence (XAI) modules. By using numerically grounded contour integration techniques within a deep learning module, CITADL detects temporal and spatial patterns in biometric signals based on adaptive fairness regularization and transparency layers, which allow it to explain the decision-making process. The framework is further supplemented through a quantum feature regeneration module that is designed to encode contour-integrated biometric representations in a Variational Quantum Circuit (VQC) and generate enhanced nonlinear correlation modelling. The resulting measured qubits features are decoded and harmoniously injected into the classical deep-learning pipeline, thus retaining the transparency, fairness and explainability. The evaluations of preliminary studies show 97% relative improvement in predictive accuracy and fairness metrics compared to selected baseline models in clinical biometric applications, thus contributing to the development of a reliable and transparent methodology for ethical augmentation of medical biometric data.

KEYWORDS: Biometric; quantum; qubit; interpretability; contour; fairness; decision-making; accuracy; gradient

1 Introduction

Today, medical biometric data have surpassed the medicine of simply diagnosing and detecting diseases and equipped the modern medical system leveraging cross-disciplinary AI techniques [1]. Patient identification using medical biometrics such as iris scans, fingerprint patterns, physiological signals, and facial recognition provides highly secure and efficient identification in the medical environment. Electronic healthcare records (EHR) management, telemedicine, and secured access control in the healthcare infrastructure make extensive use of these biometrics [2]. Along the way, however, concerns related to systemic bias and lack of model interpretability, and fairness have started to arise as well. While Deep Learning (DL) models offer high predictive capability, they often lack interpretability [3]. Considering the sensitivity and exigencies of the clinical setting mandated by components like fairness, accountability, and reliability, such non-transparent nature of biometric AI models poses challenges in clinical validation and ethical deployment [4]. Furthermore, the recent advances in quantum-enhanced learning paradigms provide new opportunities for modeling the complex non-linear dependencies using representations of high-dimensionality in Hilbert space, which in turn stimulates the concept of a hybridization of a quantum refinement mechanism within transparent deep learning architectures.

Recent research in AI-driven biometric systems has addressed the deeper evolution of DL frameworks for biometric enhancement, the notion of fairness-aware machine learning (ML), and the notion of explainable AI (XAI) frameworks [5]. The improvement of biometric recognition accuracy has been studied in the context of Convolutional Neural Networks (CNNs), Transformers, and attention-based models. Fairness-oriented approaches, e.g., reweighted loss functions, adversarial debiasing, and domain adaptation methods, are also introduced to reduce demographic bias [6]. However, these promises are mostly unfulfilled partly due to limited incorporation of formal mathematical representations like contour analysis, fairness-aware optimization, as well as transparent, robust mechanisms of biometric DL models [7,8]. Unfortunately, most of the existing approaches do not employ high-end mathematical computations like contour integral transformations to improve both the interpretability and fairness of the approach, thereby raising ethical concerns about the deployment of AI in healthcare [9,10].

This study proposes the Contour Analysis Integrated Transparent Augmented Deep Learning (CITADL) methodology to fill the void, a state-of-the-art integration of high-end contour mathematics into deep learning biometric analysis. It does so by embedding contour–based feature transformation into the context of the learning pipeline, which allows it to capture more complex biometric structures than the traditional approaches. On top of that, it includes a fairness-aware loss function and an explainability module to make sure that the predictions are accurate and explainable. The proposed CITADL framework emphasizes trustworthiness and debiasing and enables robust feature attributions in biometric decision-making. Therefore, it is used in high-risk AI-driven medical applications.

The selection of contour integral transformations is technically motivated by their ability to project biometric features into a complex-valued domain, enabling the model to capture both local and global variations through boundary-aware integration. This allows more expressive feature encoding, essential in preserving discriminative structures in physiological signals like iris textures, ECG patterns, and facial landmarks.

1.1 Research Novelty

Raw biometric features are augmented in the complex contour integrated feature space where high order spatial and temporal dependencies that are not naturally captured by traditional deep learning models are encoded. By augmenting the feature representation for the sample image, this enriches the biometric dataset and improves the robustness, fairness, interpretability [11]. A unique feature of quantum-enhanced CITADL is that it aims to increase the transparency, interpretability, security, and fairness of AI-driven biometric applications, partly preserving their security and robustness. CITADL enables bias-free patient identification in healthcare authentication systems, which decreases the misidentification risk of having unauthorized access to patients' medical records. In AI-assisted diagnostics, the framework enables explainable contributions to biometric features to inform clinicians' understanding of how biometric markers feed into disease predictions. Quantum-enhanced CITADL can be used in telemedicine and remote monitoring for biometric verification to ensure secure and fair verification of patients in such virtual healthcare platforms. In addition, enhancing the methodology of AI-based forensic biometric systems grants reliable and precise identity verifications for biometric support applications in the law enforcement sector. Contouring-integrated learning, despite augmenting representational expressivity, encounters challenges in modelling high-order cross-modal dependencies within purely classical spaces. Quantum feature maps provide a principled means of representing correlations to entanglement to allow for the ability to refine contour-derived biometric signatures compactly and nonlinearly. Accordingly, a quantum-enhanced CITADL, which remains fairness-aware and explainable, is introduced. CITADL fuses mathematical rigor with state-of-the-art AI-driven biometric learning to create an innovation in biometric AI technology that promises to be fair, interpretable, and secure for medical and security-based biometric applications. The most important contribution that the present study has made, is the smooth fusion of contour-integral feature learning with a variational quantum refinement module, thus initiating a hybrid transparent framework that can simultaneously harmonize the principle of boundary-awareness, quantum-enhanced non-linear modelling, fairness constraint, and interpretable deep authentication under one unified architectural paradigm.

1.2 Significance and Contribution

The ability to achieve high accuracy, fairness, and explainability in AI-driven medical biometric systems is essential in various healthcare and security-based applications, which is a significant contribution to the proposed quantum-enhanced CITADL framework. CITADL stands out from other traditional deep learning models because it is an opaque black-box system, but instead, it integrates mathematical contour-based transformations to give interpretable and bias-mitigated biometric decision-making with significant processes of quantum computing. In this context, this study contributes to the field by improving and mediating the development of AI's trustworthiness for medical identity verification, patient authentication, as well as biometric-aiding diagnosis. However, the framework provides robust resistance against adversarial attacks, thereby enhancing security and ethical compliance of biometric processing. To improve the transparency of model predictions and reduce demographic bias, quantum-enhanced CITADL creates a framework that enables fair AI deployment in telemedicine as well as for EHR access control and clinical data protection, thus paving the way for better medical biometric applications.

1.3 Scope and Motivation

This work can be extended to developing secure, fair, and explainable AI-generated biometric systems in any domains that are dependent on fair, secure, and XAI-driven biometric systems, especially in healthcare security, digital patient authentication, and AI-assisted clinical diagnostics [12]. The growing use of AI for patient monitoring based on biometrics and access to medical records are among the main reasons for the present research that suffers from bias and security threats and yet is not easy to universally understand. Deeply learning biometric models in the current era tend to be biased towards demographics and can lead to incorrect classification of minority groups in medical datasets, resulting in significant healthcare disparities [13]. Moreover, the lack of transparency of the systems in biometric authentication and clinical decision-making hampers medical professionals' ability to trust the AI-assisted biometric verification system. Quantum-enhanced CITADL integrates quantum computing and explainability mechanisms on contour that is fairness-aware into the learning process, ensures that biometric AI applications achieve the required levels of security, ethics, and transparency for real-world medical deployment, and thereby allows trust in AI-based tools in medical applications.

1.4 Research Objectives

The target goals of this study are as follows.

To develop and implement the CITADL framework, both contour integral mathematics and DL is combined for enhanced representation of biometric features.

To acquire the ability to integrate fairness-aware optimization methods to reduce demographic bias in biometric AI models.

To utilize Contour-Aware SHapley Additive exPlanations (SHAP) and Contour Integrated Gradients (CIG) in order to interpret biometric AI decisions and their feature attributions, which makes them more transparent and explainable.

The research work was initiated with an introduction (Section 1) that led to the Related Work segment (Section 2), which details available biometric AI models. The methodology (Section 3) provides details about data preprocessing combined with contour-integrated feature transformation, deep learning architecture, optimization techniques, and explanation mechanisms. The Materials utilized sector (Section 4) explains the dataset used, and Performance Evaluation (Section 5) explains both experimental outcomes and their analysis. Future directions and main research findings are presented in the Conclusion and Futuristic Research section of the paper (Section 6).

2 Related Works

A DL-based multi-modal biometric recognition system defined by [14] uses face along with iris and finger venous features as authentication keys to boost biometric security. The study enhances accuracy and reliability through feature fusion at different levels through CNNs. This research implements VGG-16 architecture as part of Feature and Score Level Fusion (FSLF) to merge the results from three separate CNN models, which recognize iris and face and finger vein attributes to boost identification outcomes. The main process starts by extracting features with VGG-16 pre-trained CNN, followed by image augmentation and dropout techniques for preventing overfitting and fine-tuning with Adam optimization together with a categorical cross-entropy loss function. Researchers evaluated their methods by using the multi-modal traits dataset of Shandong University ML and Applications-Human Multi-Modal Traits (SDUMLA-HMT). The research achieved 99.39% accuracy through feature-level fusion and reached 100% accuracy when using score-level fusion with product rule and arithmetic mean calculations above individual approach results. Increasing recognition accuracy became possible by merging all three biometric traits during the process. A drawback of the model is its dependency on VGG-16 since image resizing leads to detail reduction and introduces high computational complexity from deep learning needs.

Large-scale biometry research utilizing UK Biobank neck-to-knee MRI scans got its basis from [15], who developed an interpretable neural network regression framework. Research targeted the development of a standalone DL model that automatically predicts 64 biological measurements such as body composition, fat distribution, and muscle volume data. The research methodology utilizes ResNet50-Based Image Regression and Saliency Analysis (IRSA) that trains ResNet50 convolutional neural networks with two-dimensional MRI projections to forecast biological and health measurement parameters. Training different neural networks for biological metrics occurs through standardized processing, during which separate models assess each measurement. Analysis of image saliency identifies specific regions that primarily affect model prediction, making the model results easier to understand. The examination delivered results showing 0.972 median R2 scoring and 99.97% accuracy in sex determinations and 90% accuracy in liver fat level identification, which corresponded to age estimation prediction MAE of 2.46 years and visceral adipose tissue volume MAE of 140 mL. Research results demonstrated that the network achieved superior performance compared to conventional regression methods while producing outcomes better than gold-standard method agreements. The model requires additional testing for various demographic populations and imaging methods and performs its operations in two dimensions, limiting optimal measurement compatibility.

The study in [16] developed a gender classification method through behavioral biometrics by examining signed handwriting samples as physical evidence. The study investigates different methods of combining features to enhance classification results for gender identification used in biometric security and legal investigations. Migration processes for Feature Fusion-Based Machine Learning Classification (FFMLC) utilize Histogram of Oriented Gradients (HOG), Local Binary Patterns (LBP), and textural and statistical features for completing classification tasks. The study analyzes 4790 handwritten signature images to gather their features while employing concatenation for feature fusion, which then proceeds to signature classification through a Decision Tree (DT) and k-NN together with a Support Vector Machine (SVM). The study achieved 96.17% accuracy with k-NN, while DT delivered 98.72% accuracy, and SVM reached 100% accuracy. The combined use of several features through fusion processing leads to superior accuracy beyond what can be achieved by separate categorizations of individual features. The main constraining aspect of the methodology is the intrinsic limitation of the self-authored and non-diverse handwriting collection, so the system may struggle to function properly when processing flawed signature samples.

Researchers in [17] explored how physical characteristics of medical chest X-ray data present privacy concerns when deep learning re-identifies patients. Deep learning models have proven effective at re-identifying patients contained within public chest X-ray datasets, which creates an issue regarding patient privacy protection in these medical datasets. The Siamese Neural Network (SNN)-Based Patient Re-Identification system uses ResNet-50 features together with contrastive loss features for embedding similarity learning. The training process utilizes the ChestX-ray14 dataset to confirm patient associations between X-ray pairs, while retrieval-based patient re-identification depends on Euclidean distance calculations for learned embedding comparison. This research examines how well the model performs on tests using CheXpert as well as COVID-19 Image Data Collection data. The study achieved the verification of patient pairs with 95.55% accuracy and computation of 0.9940 AUC, while image retrieval reached 97.48% mAP@R and 99.63% Precision@1 results. The model maintained its effectiveness when X-ray scans were separated by twelve years. Both independent evaluations demonstrated high generalizability performance because the AUC reached 0.9870 for CheXpert and 0.9763 for the COVID-19 dataset. The model demonstrates strong accuracy, but its effectiveness depends on specific noise patterns in the dataset, and it cannot address possible biases that occur due to inconsistent metadata.

The research of [18] proposed a novel GAN-EAI (Generative Adversarial Networks (GANs) and Explainable Artificial Intelligence (XAI)) framework for generating synthetic biometric images while preserving privacy. The study effectively addresses critical challenges in biometric systems, including privacy concerns, data scarcity, bias, and regulatory restrictions, by producing high-quality synthetic data while maintaining transparency and interpretability. The incorporation of XAI enhances trustworthiness by enabling the validation and explanation of generated outputs, thereby supporting fairness, robustness, and bias mitigation. Experimental results have shown that the framework provides a function of better image quality, better level of privacy protection, and reduced data bias that can be used for applications such as authentication, health care, and identity verification. The study, however, seems to lack discussion on scalability to various biometric modalities, computational complexity, and deployment challenges, which may warrant further investigation.

Authors in [19] presented a visual-textual explanation framework for biometric verification systems that use piece-wise facial attribute analysis techniques. The research project establishes an enhanced interpretation of biometric verification through facial component analysis while generating visual explanations and textual descriptions of verification results. The implementation relies on Uniform Manifold Approximation and Projection (UMAP)-Based Facial Attribute Representation with XAI (FAR-XAI), which merges Mask R-CNN image segmentation with Autoencoder feature extraction and utilization of UMAP for dimension reduction and Long-Short Term Memory (LSTM) for automatic description production. The fundamental phases of the process include dividing facial components into segments, followed by their representation in a latent dimension space before performing UMAP-based difference visualization between subjects. A CNN-LSTM model uses its architecture to create textual descriptions of face features that differentiate the subjects. This study reached two significant achievements through its methods, including a genuine/impostor verification success rate of 89% and a 90% classification rate using four-component UMAP representations as well as a text-to-image correlation above 70%, which combined reaches an overall accuracy of 154%. This study achieves better transparency in biometric verification systems through the connection of textual explanations to image-based explanations. The segmentation process depends on color tones, which leads the model to recognize challenges when processing images with high contrast and produces occasional wrong feature connections because of annotation mistakes found in the dataset and its uneven attribute distribution.

Investigators in [20] introduced an AI-powered DL model for multi-modal biometric fusion as a solution to boost recognition accuracy together with generalization in public security applications. This research merges biometric verification through score-level fusion and a combination of feature-level fusion and pixel-level fusion using DNNs. This research uses DNN-Based Multi-modal Biometric Fusion (MBF) that implements pixel-level channel and spatial and intensity fusion together with feature-level modality-specific branches and joint representations and score fusion methods based on Rank-1 evaluation and modality ranking. The main process merges fingerprint, face, and iris modalities while optimizing representation training and backpropagation to enable feature dependency refinement. The data collection consists of 2712 subjects who provided 40,482 biometric images to mimic actual system degradation effects. The research study delivered three main achievements: 2.2% higher accuracy from multi-modal feature fusion along with 3.5% better retrieval accuracy from score fusion while achieving 99.6% overall system accuracy. The combined multi-modal fusion algorithm delivered superior results to single-modal algorithms, thus proving its strength for practical use cases. The model has restricted use since it demands retuning procedures for diverse population demographics and imaging task conditions, while pixel-level unification fails to boost retrieval effectiveness.

The work in [21] developed an auditing system for machine learning databases that focuses on ensuring fair, privacy-preserving, and legally compliant biomedical and healthcare information. A comprehensive analysis of more than one hundred datasets measures privacy risks, fairness standards, and legal norm compliance to prevent irresponsible AI behavior. Responsible Rubric-Based Dataset Evaluation (RRDE) serves as the selected methodology for data assessment through its three fundamental evaluation components. The three key dimensions of dataset evaluation include privacy, fairness, and regulatory compliance, which measure sensitive attribute presence together with inclusivity, diversity scores, and label reliability and institutional approval, consent, and data removal options, respectively. The method analyzes 60 healthcare and biometric datasets according to these criteria before calculating a representative three-dimensional dataset responsibility score to detect curational weaknesses. The study demonstrates average findings, with fairness scoring 0.96 points out of 5 points, privacy assessment reaching 4.5 points out of 6 points, and regulatory compliance reaching 0.58 points out of 3 points. Among the considered datasets, UTKFace demonstrated maximum fairness responsibility at 2.71, while FB Fairness Dataset obtained the highest total responsibility score. This study demonstrates the fairness–privacy paradox through its documentation that improving fairness by adding sensitive attributes requires greater protection of privacy. The main drawback of the framework involves its inability to assess biases outside demographic categories, and its manual evaluation method hinders automation for privacy assessment.

Authors in [22] developed a DL-based forensic iris segmentation system for postmortem identification by building a recognition system that identifies the biometric traits of deceased individuals. The investigation focuses on solving iris pattern recognition for deceased individuals because this recognition affects legal procedures and forensic investigations. The system uses the Triplet Loss Postmortem Iris Model (TLPIM), which combines Mask R-CNN for segmentation with a deep learning ResNet-50-based model designed for feature extraction and matching. The core operation starts with Mask R-CNN detection of the iris annulus together with decomposition artifacts before extracting features through TLPIM. CAM creates visual depictions through which forensic examiners receive assistance with their investigative choices. The research findings demonstrate an 88.38% (Intersection over Union) segmentation accuracy and a recognition accuracy (AUROC) of 0.95 for pictures acquired within the first 24 h after death. Additionally, it achieved an overall recognition performance of 0.89 AUROC. The main drawback of this approach is that recognition rates decrease as the amount of time between death and sample analysis extends.

The research in [23] examined biometric pattern privacy measures by employing XAI and synthetic data for analysis. The research works to decrease biometric data transmission recognition challenges by uniting synthetic data generation approaches with explainable AI systems. The main process makes synthetic biometric data through AI-based interpretable methods to secure privacy while minimizing security threats. The use of convolutional filters reduces interpretability problems by enhancing biometric pattern recognition while improving image features. The system incorporates a decision-processing unit that delivers accurate recognition results with minimal false acceptances. The study reached three significant objectives, including an 89% flow efficiency combined with 96% data accuracy and a 1% limitation in data transformation errors. Security, along with biometric recognition reliability, reached new heights due to these significant enhancements. One drawback of this approach involves synthetic data security enhancement, which causes model robustness to decrease by 4%, along with an increase in model complexity by 6%. Table 1 represents the overall summarized view of all the existing approaches.

Table 1: Summarized overview of existing studies.

References	Methodology	Components	Attainments	Limitation
[14]	VGG-16+ FSFL	Deep learning-based multimodal biometric recognition using iris, face, and finger vein	99.39% (feature-level fusion), 100% (score-level fusion)	Image resizing may cause feature loss; high computational cost
[15]	ResNet50+ IRSA	Automated biometry using deep learning on UK bio-bank MRI data with interpretable saliency mapping	R^2 = 0.972, 99.97% sex classification accuracy, 90% liver fat detection accuracy, MAE of 2.46 years (age) and 140 mL (VAT)	Lacks an independent test set; requires retraining for different demographics and imaging protocols
[16]	FFMLC	Offline handwritten signature-based gender classification using LBP, HOG, statistical, and textural features	96.17% (k-NN), 98.72% (Decision Tree), 100% (SVM)	Dataset lacks diversity; performance may degrade with low-quality signatures

(Continued)

Table 1 (continued)

References	Methodology	Components	Attainments	Limitation
[17]	SNN-PRID	Deep learning-based verification and re-identification of patients using chest X-ray embedding	AUC = 0.9940, 95.55% classification accuracy, 97.48% mAP@R, 99.63% precision@1	Relies on dataset-specific noise; does not address metadata biases
[18]	GAN-EAI Framework	GANs; XAI Techniques; Privacy-Preserving Mechanism; Bias Mitigation Module; Synthetic Biometric Dataset	High-Fidelity Image Synthesis, Interpretability, Enhanced Privacy, Trustworthy Biometrics	Computational Overhead; Scalability Concerns, Modality Generalization Unclear, Limited Real-World Validation.
[19]	UMAP+ FAR-XAI	Visual and textual explainability for biometric verification via facial feature segmentation and semantic mapping	89% verification accuracy, 90% with four-component UMAP, 70% alignment of textual and visual attributions	Dataset annotation errors cause occasional misattributions; struggles with black-and-white images
[20]	DNN+MBF	AI-based fusion of face, fingerprint, and iris data for enhanced biometric security	2.2% accuracy gain (feature fusion), 3.5% accuracy gain (score fusion), 99.6% overall accuracy	Requires retraining for different demographics; pixel-level fusion has minimal impact
[21]	RRDE	Fairness, privacy, and regulatory assessment of biometric and healthcare datasets	Fairness: 0.96/5, Privacy: 4.5/6, Regulatory: 0.58/3	Does not account for dataset biases beyond demographics; manual privacy annotation limits automation
[22]	TLPIM	Deep learning-based postmortem iris segmentation and recognition with explainable AI for forensic use	88.38% segmentation accuracy (IoU), AUROC 0.95 (<24 h), AUROC 0.89 (overall)	Slightly lower recognition accuracy than existing methods; performance declines with increasing postmortem interval
[23]	XAI-based Synthetic Data Generation	Integration of synthetic biometric data with XAI to enhance privacy and security	89% flow efficiency, 96% accurate synthetic data generation, 1% transformation error	Reduced robustness by 4%, increased complexity by 6%

Quantum-assistive machine learning (Q-ML) has recently fathomed in the areas of variational classifiers, kernel learning, and feature embeddings when the unlikely correlations and the compressed representations are favorable. Nevertheless, Q-ML has rarely been combined with formal contour-integral feature construction or fairness-constrained, explainability-driven processing pipelines, which is the primary motivation for the addition of a variational quantum refinement layer after contour transformation and then before the deep attention network.

3 Methodology

Contour-Integrated Transparent Augmented Deep Learning (CITADL) methodology adopts a structured five-stage process for improving fairness, interpretability, and robustness in medical biometric analysis. Fig. 1 depicts the complete pipeline of CITADL procedures. In the beginning (stage 1), the preprocessing and feature normalization stage reduces raw biometric inputs into a standardized format to make them numerically stable and consistent for various demographic groups. Then, in stage 2, the Contour Integral Feature Transformation (CIFT) projects the biometric features into a high-dimensional complex space by contour integral computations that facilitate the exploitation of complex spatial and temporal dependencies. Located between CIFT and CITDNN, the Quantum Contour Feature Encoding and Variational Quantum Refinement (QCFE-VQR) module is responsible for the refinement of contour-aware feature representations by quantum encoding, variational transformation and measurement, before directing them to the next deep learning stage.

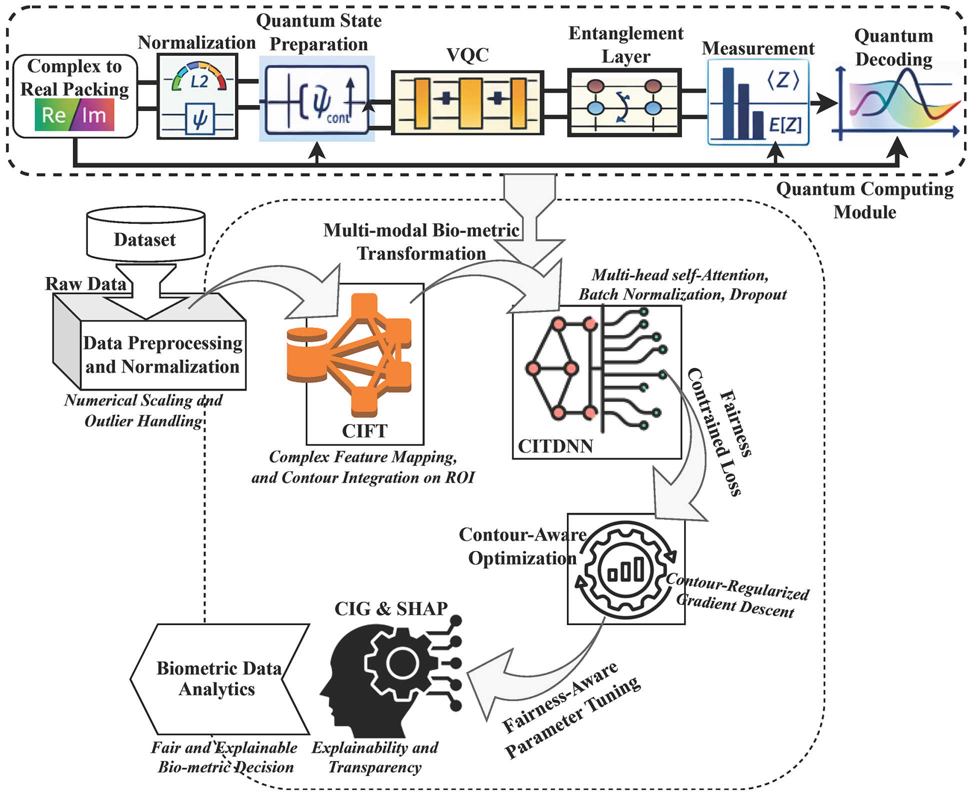

Figure 1: Architecture of CITADL methodology.

Stage-2 features are additionally encoded and refined via a variational quantum circuit before entering CITDNN. In stage 3, the Contour Integrated DNN (CITDNN) is a powerful multi-headed network consisting of multi-head attention, batch normalization, and dropout layers that is applied to further refine the feature representations obtained in stage 2, while fairness constraints avoid unfairness in inference decisions. In order to improve learning, stage 4, Contour aware stochastic gradient descent, a stage in which adaptive gradient updates are applied in order to preserve the numerical stability of contour-integrated features while accelerating convergence, is applied. Thirdly, stage 5 finally completes our explainability and transparency stream via Contour Integrated Gradient (CIG), where integrated gradient and contour-informed SHAP values are used to determine the interpretability and counterpart the biometric key features and their corresponding contributions towards the respective model prediction and hence, to provide a transparent decision-making process. This structured pipeline enables enhanced improvements in predictive accuracy and fairness to improve model performance in releasing reliable and ethically sound biometric AI applications.

3.1 Data Preprocessing and Normalization

The preprocessing of raw biometric data D, aimed at ensuring stability, consistency, and fairness in subsequent DL operations, is the first step in the computational workflow. First, structured feature vectors are created from biometric features. The raw feature vectors in these typically had variations induced via environmental factors, sensor noise, or among individuals. Normalization techniques are used to normalize all features to a uniform scale to deal with such inconsistencies. The preprocessed feature $\left(X_i^{'}\right)$, for given a medical biometric dataset D that contains samples S with biometric feature vectors $\left(x_i \in \mathbb{R}^d\right)$, respective labels (y_i), and sensitive attributes (a_i) is expressed as,

$$X_i^{'} = (x_i - m/\Delta) \tag{1}$$

From (1), m and Δ denotes the mean and variance of each x_i, respectively. This process is performed in order to ensure numerical stability and feature scaling. To remove the domination of some features over others for their training, each feature is standardized across the dataset using mean subtraction and standard deviation scaling. The key to obtaining a optimal convergence for the model, better numerical stability, and the preservation of biometric variations uncorrupted by distortions lies in this preprocessing phase.

3.2 Feature Transformation

After normalizing biometric features $\left(X_i^{'}\right)$, they are fed into a higher-dimensional complex space through contour integral transformations which is referred as Contour Integral Feature Transformation (CIFT) [24].

$$\mathcal{Z}_i = \text{Ҭ}\left(X_i^{'}\right) + i \cdot l\left(X_i^{'}\right) \tag{2}$$

From (2), $l\left(X_i^{'}\right)$ represents the learned non-linear transformations. A simplified example of Eq. (2) can be shown using a biometric feature vector x = [1, 2] and a circular contour Υ (example, $z = e^{i\theta}, \theta \in [0, 2\pi]$). Let the kernel be $k(x, y) = z + 2z^2$. Then the contour integral becomes $\phi(x_i) = \int_\Upsilon \left(z + 2z^2\right) dz = 0$. Thus, by using integral theorem, only the coefficient of z^{-1} contributes a nonzero value in a closed contour integral (residue theorem). Since there is no z^{-1} term here, the integral becomes zero, unless the kernel is designed with inverse powers or singularities.

Further, this CIFT stage integrates contour integration as an alternative to traditional linear, non-linear projections by capturing advanced spatial, structural, and temporal biometric data dependencies, which is computed as,

$$\phi(x_i) = \frac{1}{2\pi i} \oint_{\Gamma(\mathcal{Z}_i)} \frac{l(\gamma, \delta; \omega)}{\delta^2 + (\omega - \delta)^2} d\omega \tag{3}$$

From (3), $\Gamma\left(\mathcal{Z}_i\right)$ denotes the enclosing contour on the Region of Interest (RoI) in the given complex plane, $l(\gamma, \delta; \omega)$ indicates the learned attributes of complex kernel of each feature in order to capture spatio-temporal dependencies, and the expression, $\delta^2 + (\omega - \delta)^2$ signifies the regularization term (ensuring numerical stability). In practice, numerical approximation of the contour integral is computed using discrete sampling over the ROI in the biometric image (e.g., iris boundary). The biometric feature map is treated as a 2D surface f (x, y), and integration is applied over the closed pixel boundary (the contour) using a discrete summation, $\sum_{(x_k,y_k)\in} f(x_k, y_k) \cdot \Delta s_k$ (where Δs_k segment length on the contour path).

Using complex plane mappings of real-valued biometric features enables the model to discover hard-to-abstract relationships that standard methods cannot acquire. Complex feature kernels strengthen the representation capabilities by helping the system achieve better discrimination of subtle biometric variations. Prior to DL model input, biometric signals must undergo an optimal transformation during this vital stage because they tend to display non-linear patterns. Contour-based representations increase the feature expressivity of the biometric system to improve its resistance against variations and maintain important identity data.

3.3 Quantum Contour Feature Encoding and Variational Quantum Refinement (QCFE-VQR)

The contour integrated feature vector is additionally encoded into a quantum Hilbert space by amplitude encoding, which reflects the quantum state encoding of biometric information $|\psi(x)\rangle$ and its core computation is defined as,

$$|\psi(x)\rangle = \sum_{j=0}^{2^q-1} \frac{r_j(x)}{\sqrt{\sum_{k=0}^{2^q-1} |r_k(x)|^2}} |j\rangle \tag{4}$$

In Eq. (4), the real-valued contour representation, $\phi(x_i)$ is referred as $r(x)$, q indicates the number of qubits utilized for encoding, 2^q represent the quantum Hilbert space dimension. This computation shows that the boundary aware biometric features are mapped coherently to a quantum state. The trade-off between quantum features resolution and computational overhead is governed by the number of qubits (q), with larger q providing better representational fidelity to contour features but implying higher resource requirements (and smaller q providing amenable performance to deployment).

So, to improve the non-linear contour interactions from the classical transformation, a VQC is used on the encoded state.

$$|\psi_\theta(x)\rangle = U_{VQC}(\theta) \Rightarrow \prod_{l=1}^{L} \left[U_\varepsilon^{(l)} \prod_{k=1}^{q} \left(\mathbb{R}_y \left(\theta_k^{(l)} \right) \cdot \mathbb{R}_z \left(\theta_k^{(l+1)} \right) \right) |\psi(x)\rangle \right] \tag{5}$$

In Eq. (5), $U_{VQC}(\theta)$ refers the trainable unitary of VQC, L signifies the count of variational layers, $U_\varepsilon^{(l)}$ indicate the entangling function, θ denote the set of quantum (learnable) parameters, and $\mathbb{R}_y$ and $\mathbb{R}_z$ both highlights the single-qubit rotation gates.

The refined quantum state is measured for extracting expectation values, which is then concatenated with the classical contour features that are fed-in at the CITDNN block.

$$z_x(x) = \left\langle \psi_\theta(x) \middle| \rho_z^{(k)} \middle| \psi_\theta(x) \right\rangle, where\ \phi(x_i) \leftarrow z_x(x)\ and\ k = 1, \cdots, q \tag{6}$$

In Eq. (6), $\psi_\theta(x)$ is the trained quantum state from Eq. (5), $\rho_z^{(k)}$ signifies the Pauli-Z observable on kth qubit, $z(x)$ is the quantum feature vector returned to classical approach. For decoding, the measured quantum expectation values are transformed via a structured post-measurement transformation to obtain a stable, noise-tolerant classical feature representation for subsequent fairness-aware, deep learning and optimization. Both encoding and decoding are practically performed in step-wise manner:

- Amplitude encoding (contour-integrated feature vectors) encode feature amplitudes into qubit probability amplitudes, normalizing and encoding the feature vectors into quantum states.
- The measured expectation values of Pauli observables decodify the refined quantum states, and post-process to stable classical feature vectors to be used as inputs to downstream learning.

Variational quantum circuit is an extension of nonlinear correlation modeling to directly map contour-integrated features to high-dimensional Hilbert space where feature interactions, in all combinations, are modeled by quantum superposition and entanglement. This allows the model to learn higher-order dependencies which do not lend themselves to learning in classical feature spaces, thus enhancing representational richness and accuracy in decision-making.

3.4 Contour-Integrated DNN

The contour-integrated descriptors are then passed to QCFE-VQR, which returns measured quantum features that are subsequently utilized by the Contour-Integrated DNN (CITDNN). The CITDNN [25] employs multiple layered DNN (L_θ) processing of extracted transformed biometric features $\phi(x_i)$ for achieving fair interpretable and robust system performance, which is expressed as,

$$\hat{y}_i = L_\theta(\phi(x_i)) \tag{7}$$

In (7), $L_\theta(\cdot)$ denotes the network operates under θ parameters, which get optimized through the contour-regularized loss function which is computed as,

$$\mathbb{L}(\theta) = \frac{1}{N}\sum_{i=1}^{S} \mathbb{L}_{\text{¢}}\left[L_\theta(\phi(x_i)), y_i\right] + \alpha_1 \cdot \mathfrak{q}_{CI}(\theta) + \alpha_2 \cdot \mathfrak{q}_F(\theta) \tag{8}$$

From (8), the smoothing of transformations is performed via contour-integral regularization, $\mathfrak{q}_{CI}(\theta)$ (attained via Eq. (9)) and $\mathfrak{q}_F(\theta)$ provides demographic fairness for prediction results (attained via Eq. (10)) with cross entropy loss (Eq. (11)).

$$\mathfrak{q}_{CI}(\theta) = \frac{1}{2\pi i}\sum_{i=1}^{S}\left(\oint_{\Gamma(\zeta_i)}\left|\frac{\partial L_\theta(\omega)}{\partial\omega}\right| d\omega\right) \tag{9}$$

$$\mathfrak{q}_F(\theta) = \left\| E_{\mathfrak{S}}\left[L_\theta(\phi(x_i)) \mid \mathfrak{S} = 1\right] - E_{\mathfrak{S}}\left[L_\theta(\phi(x_i)) \mid \mathfrak{S} = 0\right]\right\|^2 \tag{10}$$

From Eq. (10), $E_{\mathfrak{S}}[\cdot]$ determines the expected prediction for each of the sub-group $\mathfrak{S}$.

$$\mathbb{L}_{\text{¢}} = -\sum_{i=1}^{S}\left[(1-y_i)\ log\ (1-\widehat{y_i})\right] + y_i \cdot\ log\ (\widehat{y_i}) \tag{11}$$

Eq. (10) computes the expected subgroup-wise prediction deviation, acting as a fairness penalty term that measures disparities among sensitive attributes (e.g., gender, ethnicity). This term is integrated into the overall loss function in Eq. (11) along with cross-entropy loss, enforcing the model to minimize prediction variance across subgroups. Subgroup-wise prediction deviation (demographic parity) is used to measure fairness, both applied to sensitive attributes and assessed by Fairness Aware Performance Metrics (FAPM). It is imposed on training by adding a fairness regularization term into the loss, which causes the model to reduce prediction differences among demographic groups. As a result, the model is guided not just by accuracy but by demographic parity, effectively reducing overfitting to dominant groups. The impact is empirically validated in the evaluation, where CITADL consistently achieves the lowest Fairness Gap (FAPM ~0.012) across 15 demographic groups, confirming the practical success of these fairness constraints in mitigating bias.

Dense layers apply multiple processing steps to the extracted contour-integrated features through Leaky-ReLU activation in order to prevent gradient vanishing [26]. The multi-head self-attention layers develop dynamic weight systems that emphasize important biometric areas to maintain essential details after removing excess variation. Learning stabilization is attained through batch normalization within the deep architecture, whereas dropout layers avoid overfitting issues. A fully connected layer system operates as the main decision-making unit before the model reaches its final class output. The biometric AI system with combination of contour mathematics and DL produces stronger resilient results that are transparent and accurate while enhancing fairness through decision interpretation and vulnerability reduction.

3.5 Contour-Aware Optimization

A DL model requires training with the optimization mechanism known as Contour-Aware Stochastic Gradient Descent (CA-SGD). Standard gradient-based optimizers such as Adam face difficulties when dealing with complex feature spaces that result from contour-integrated transformations. The platform CA-SGD includes adaptive learning updates that maintain stable numerical values of contour-based features to optimize model training processes [27]. The optimization process makes use of adaptive gradient clipping to stop overfitting by maintaining model sensitivity to small changes in biometric data. The core computation part of CA-SDG in the process of convergence and complex gradients is expressed as,

$$\theta^{(t+1)} = \theta^{(t)} - \left[\mathbb{L}\left(\theta\right) \cdot \nabla_\theta + \frac{1}{2\pi i}\left(\oint_{\Gamma(z_i)} \left|\frac{\partial L_\theta\left(\omega\right)}{\partial \omega}\right| d\omega\right)\right] \cdot \varphi \tag{12}$$

From Eq. (12), $\mathbb{L}\left(\theta\right) \cdot \nabla_\theta$ signifies the core complex gradients whereas φ denote the learning rate. Momentum-based acceleration methods integrated into the learning process speed up convergence and create well-behaved decision boundaries. This stage ensures effective training that avoids both instability and fairness violations. Thus, the DNN produces ethical and reliable predictions for biometrics.

CA-SGD has been developed to help deep learning models perform better in spaces where the usual optimizers are usually ineffective due to their unusual geometry and highly bent slopes. When SGD methods are used with CITADL, their assumption of linear gradients and Euclidean space no longer applies, leading to problems. CA-SGD adds the detailed curves from contour maps to the procedure for optimizing neural networks. The optimizer adapts the learning rate according to how bendy the contour is at a position, which helps keep the training process steady in areas with a lot of variation. In the implant region, gradient clipping in complex space constrains gradients that rise in a swift manner without features, helping the network converge with fewer issues.

It also comes with a momentum mechanism that is custom-fitted to the way the environment changes. Unlike the fixed-momentum methods, it automatically varies according to the angle and magnitude of the complex gradients. As a result, training is more stable and keeps oscillations at bay, which is valuable for working with biometric data that varies by mode and time.

In CA-SGD, curvature in the complex feature space is approximated by the magnitude and directional variation of obtained complex gradients on the basis of contour-integrated transformation. In particular, local curvature is estimated as a difference between the norm changes in gradients and phase shifts between consecutive iterations, which reflects the change in geometry of the loss surface in the complex space. It can then be utilized in learning the curvature estimates leading to a learning rate adaptation, gradient clipping, and a stable convergence in very non-linear contour-integrated spaces.

3.6 Explainability and Transparency

Interpreting decision-making in biometric AI systems is one of the key challenges to address, as the decision-making process should be interpretable by the clinician and end users. In order to mitigate such issues, this final stage is augmented with specialized explainability mechanisms that explain how predictions were made. In order to do this, the system uses contour integrated gradient based techniques to highlight features most contributing to that decision in a given biometric decision. Therefore, contour integrated gradients (CIꞬ) in the contour integrated space are computed as [28],

$$CI\mathcal{G}\left(x_i\right) = \left(x_i - \overline{x}\right) \int_0^1 \left(\frac{\partial L_\theta}{\partial x_1}, \frac{\partial L_\theta}{\partial x_2}, \cdots, \frac{\partial L_\theta}{\partial x_d}\right) \cdot L_\theta \left[\rho \left(x_i - \overline{x}\right) + \overline{x}\right] d\rho \tag{13}$$

From Eq. (13), $\left(\frac{\partial L_\theta}{\partial x_1}, \frac{\partial L_\theta}{\partial x_2}, \cdots, \frac{\partial L_\theta}{\partial x_d}\right)$ signifies the partial derivatives of L_θ, $\overline{x}$ is acting as a reference point of biometric feature vector. To achieve interpretability, contour-aware SHAP [29] is used to attribute model predictions to biometric features while keeping the complex-valued contour integrated transformations. With this, the contour-integrated DL framework is quantified to ensure fair and transparent decision-making. Furthermore, the contour-aware SHAP $(\mathfrak{h})$ values are computed as,

$$\mathfrak{h}\left(x_i\right) = \sum_{\mathfrak{N} \subseteq I} \left\{ \left(\frac{|\mathfrak{N}|! \left(|I| - |\mathfrak{N}| - 1\right)!}{|\mathfrak{N}|!} \right) \left[L_\theta \left(\phi\left(x_i\right)\right) - L_\theta \left(\phi\left(\overline{x}\right)\right) \right] \right\} \tag{14}$$

From Eq. (14), based on the prediction accuracy test, $\mathfrak{N}$ is a subset of features that measures their contribution to the model's prediction. The model has the full set of input features, which is denoted by I.

Beside the regular computations, Computing Contour-Augmented Explainability Score [30] (CAES) is essential to quantify the interpretability of the model prediction by including contour-based gradient in explainability metrics. This process uses integrated gradients to render the sensitivity of contour transformations while ensuring the most influential biometric features are showcased with high transparency. CAES computes the gradient magnitudes along the contour-integrated feature space to provide a reliable measure of feature attribution and improve the trustworthiness of the medical biometric AI model.

The reliability of the model and its prediction grounded in biometric meaningful attributes as opposed to irrelevant artifacts can be verified with the help of this explainability layer. Additionally, fairness evaluation is performed by assessing the disparity in the model's decisions for different subgroups to avoid systemically wrong predictions by the model. This stage harnesses explainability mechanisms in order to ensure that the biometric AI system intuitively works, which fits well to be employed in mission-critical applications such as medical diagnosis and secure authentication. Table 2 represents the complete procedures of proposed CITADL approach in an algorithmic way.

Table 2: Algorithmic procedures of CITADL methodology.

Input:	
$D = \left\{\left(x_i \in \mathbb{R}^d\right), y_i, s_i\right\}_{i=1}^{S}$	*//biometric medical dataset*
m and Δ	*//feature normalization attributes*
q (number of qubits utilized for encoding), $\vert\psi\rangle$*: quantum states,* $U(\cdot)$*: Unitary Operator*	
$\Gamma\left(\zeta_i\right)$, $l\left(\gamma, \delta; \omega\right)$	*//contour transformation parameters*
$\alpha_1, \alpha_2, \theta \in \mathbb{R}^p$	*//deep learning parameters of variational quantum circuit*
φ, *ψ (iteration), τ*	*//learning rate, convergence threshold*

(Continued)

Table 2 (continued)

M_k	*//measurable operator on qubit k*
$z_i \in \mathbb{R}^m$	*//measured quantum feature vector returned to pipeline*
$g_\theta(\cdot)$	*//quantum feature map defined by the VQC measures*
Output:	
$L_{\theta^\dagger}(\phi(x))$	*//trained model*
CAES, $\mathfrak{q}_F(\theta)$	*//fairness and explainability scores*

BEGIN

1: $X_i' = \left(\frac{x_i - m}{\Delta}\right), where\ \forall i \in \{1, \cdots, S\}$ *//Feature normalization*

2: $\mathfrak{Z}_i = \mathbb{T}\left(X_i'\right) + i \cdot l\left(X_i'\right)$ *//CIFT*

3: $(x_i) = \frac{1}{2\pi i} \oint_{\Gamma(\mathfrak{Z}_i)} \frac{l(\gamma, \delta; \omega)}{\delta^2 + (\omega - \delta)^2} d\omega$ *//Capturing Spatio-temporal dependencies*

4: $\hat{y}_i = L_\theta(\phi(x_i))$ *//Contour-Integrated DNN*

with

4.1: $\mathbb{L}(\theta) = \frac{1}{N} \sum_{i=1}^{S} \mathbb{L}_{\mathbb{C}}[L_\theta(\phi(x_i)), y_i] + \alpha_1 \cdot \mathfrak{q}_{CI}(\theta) + \alpha_2 \cdot \mathfrak{q}_F(\theta)$ *//Contour Integral Loss function*

4.1.1: $\mathfrak{q}_{CI}(\theta) = \frac{1}{2\pi i} \sum_{i=1}^{S} \left(\oint_{\Gamma(\mathfrak{Z}_i)} \left|\frac{\partial L_\theta(\omega)}{\partial \omega}\right| d\omega\right)$ *//Contour regularization*

4.1.2: $\mathfrak{q}_F(\theta) = \left\| E_{\mathfrak{s}}[L_\theta(\phi(x_i)) | \mathfrak{s} = 1] - E_{\mathfrak{s}}[L_\theta(\phi(x_i)) | \mathfrak{s} = 0] \right\|^2$ *//Fairness Constraint*

4.1.3: $\mathbb{L}_{\mathbb{C}} = -\sum_{i=1}^{S} [(1 - y_i)\log(1 - \widehat{y_i})] + y_i \cdot \log(\widehat{y_i})$ *//Cross-entropy loss*

5: $\theta^{(t+1)} = \theta^{(t)} - \left[\mathbb{L}(\theta) \cdot \nabla_\theta + \frac{1}{2\pi i}\left(\oint_{\Gamma(\mathfrak{Z}_i)} \left|\frac{\partial L_\theta(\omega)}{\partial \omega}\right| d\omega\right)\right] \cdot \varphi$ *//Gradient Computation* via *CA-SGD*

6: **IF** $\left|\mathbb{L}(\theta)^{t+1} - \mathbb{L}(\theta)^t\right| < \tau$, **THEN** stop *//convergence check*

 # Computation for Explainability

7: $\mathrm{CI\mathfrak{g}}(x_i) \leftarrow (x_i - \overline{x}) \int_0^1 \left(\frac{\partial L_\theta}{\partial x_1}, \frac{\partial L_\theta}{\partial x_2}, \cdots, \frac{\partial L_\theta}{\partial x_d}\right) \cdot L_\theta[\rho(x_i - \overline{x}) + \overline{x}] d\rho$ *//via CIG*

8: $\sum_{\mathbb{N} \subseteq I} \left\{\left(\frac{|\mathbb{N}|!\,(|I| - |\mathbb{N}| - 1)!}{|\mathbb{N}|!}\right)[L_\theta(\phi(x_i)) - L_\theta(\phi(\overline{x}))]\right\}$ *//via SHAP*

9: **Compute** CAES

$= \frac{1}{N} \sum_{i=1}^{S} \left(\oint_{\Gamma(\mathfrak{Z}_i)} \left|\left(\frac{\partial L_\theta}{\partial x_1}, \frac{\partial L_\theta}{\partial x_2}, \cdots, \frac{\partial L_\theta}{\partial x_d}\right) \cdot \mathrm{CI\mathfrak{g}}(x_i)\right| dx\right)$

10: $L_{\theta^\dagger}(\phi(x))$, CAES, $\mathfrak{q}_F(\theta)$

END

For the proposed methodology with *S* number of biometric samples, *d* feature dimensionalities and ψ number of iterations; exhibits overall computational complexity of *O(Sd2ψ)*. Table 3 represents the computational complexity involved in the regular operations of CITADL. Mostly, the influence behind such complexity is CIFT and CITDNN, both of which, when added to a regular network, give more explanatory information. Typically, VGG-16 and ResNet50, which are regularly used in biometric systems, have an *O(S·d· ψ)* or *O(S·d·log d)* complexity, depending on the type of convolutional and fully connected layers in them. Fairness regularization, advanced ways of transforming features, and interpretability are not included, so these models are simpler to run, though this means they suffer from less fairness, robustness, and transparency. On the other hand, CITADL's overhead is larger as it includes the Contour-aware fairness regularization and relies on the explainability methods that make it easy to understand, but it needs additional computations during training. The computational complexity of the quantum module (QCFE-VQR) is $O(S \cdot q \cdot L)$, where q is the number of qubits and L is the number of variational circuit layers, accounting for parameterized gate operations and measurements.

Table 3: Computational complexity of CITADL algorithmic procedures.

Core Algorithmic Components	Computational Complexity	Remarks
Feature Normalization	*O(Sd)*	Each feature is standardized
CIFT	*O(Sd2)*	Requires numerical integration along complex contours it is due to the pairwise computations in the feature space
CITDNN	*O(Sd2)*	Processes data through multi-head self-attention layers it is due to matrix multiplications
CA-SGD	*O(Sd2ψ)*	Gradient computation and contour-based regularization
CIG and SHAP	*O(Sd2)*	Marginal overhead but remains bounded
Overall (CITADL)	*O(Sd2ψ)*	

Nevertheless, this computational overhead translates to significantly enhanced performance in fairness (FAPM), interpretability (CAES), and robustness, which are critical for ethical deployment in medical biometrics. When executed on GPU-accelerated systems, CITADL maintains practical runtime feasibility even with its higher complexity. Additionally, the model benefits from batch-level parallelization, and gradient clipping strategies are employed to ensure stability without exponential growth in runtime.

The optimal execution complexity leads to high scalability and operational efficiency in medical biometric datasets of various dimensions. The optimized complexity finds an excellent balance between computational feasibility and precision which makes the system suitable for real-time biometric operations.

The computed final CAES score is an average of the normalized attribution scores of the CIG and SHAP across all features with equal contribution by both approaches. The given aggregation gives a single and consistent measure of explainability, which simultaneously measures sensitivity via gradients and consistency of feature contributions.

4 Materials Utilized

The quantitative evaluation of the study depends on a high-performance computing environment to enable efficient processing of contour integrated feature transformation, DL training, and explainability computational processes. The hardware setup is a GPU-enabled system (with at least NVIDIA A-100, 40 GB) running accelerated DL computations, CPU (with at least 16 cores, AMD Ryzen-9 9900X) for general processing, 64 GB RAM for storing large biometric datasets and 2-TB NVMe SSD for model storage and fast data access. The operating system used is Ubuntu 22.04 LTS, the main programming language is Python v3.8.0, and the necessary DL framework is PyTorch v2.0 for the model training and optimization. The SciPy v1.10, NumPy v1.24, and SymPy v1.12 are included for the mathematical computations of contour integral transformations and fairness aware regularization. The biometric image is processed using OpenCV 4.7, and data handling and preprocessing are done using Pandas v1.5.3. SHAP v0.42 and Captum v0.6 are used for explainability analysis, and AI Fairness 360 (AIF360) 0.6.0 is used for fairness. Optuna v3.1 is used for model training and hyperparameter tuning. CUDA v11.8 and cuDNN v8.6 are installed for GPU acceleration to guarantee high-performance execution. For the quantum module, simulations are used in Qiskit Aer, on the same stack of GPUs. On hardware, it is configure using q-logic qubits with R measurements, shots per batch. The proposed CITADL model, trained on the hardware-software combination described in this study, verifies the efficiency of the training, evaluation, and validation, allowing for the possibility of implementing the model in scalable, real-time biometric authentication and fair AI deployment.

Simulation of realistic quantum and biometric noises is achieved by adding Gaussian noise to amplitude-coded contour features, making slight rotational variations of parameterized quantum gates, and adding depolarizing noise during measurement. Quantum Contour Fidelity Robustness (QCFR) is then computed as the mean value of fidelity between original and perturbed quantum states which measures the resilience of contour-integrated representations to such controlled perturbation.

Dataset

The proposed CITADL model is primarily evaluated using the biomedical biometric dataset [31] available in IEEE dataport for the purpose of benchmarking predictive accuracy, fairness, as well as explainability. The database contains 10,000 entries collected from a variety of 23 patients of different demographics, biometric profiles, and medical histories, rendering it ideal for model testing on real-world biometric variations. The biometric dependencies of the dataset, such as iris texture complexity, pupil dilation response, facial landmarks accuracy, fingerprint ridge density, ECG wave pattern variance, and voice pitch variability, are directly used in feature transformation due to the contour integrated mathematical encoding, proving the effectiveness of using CIFT to capture complex biometric dependencies. Moreover, the time-series nature (2022–2023) of the test folds enables evaluation of the model's capacity to adjust to biometric changes over time and be robust to longitudinal authentication scenarios. Including medical conditions in the dataset also adds value to investigating the effect, health variations have on biometric feature distributions in the context of fairness-aware optimization. This allows us to directly relate to the biometric verification accuracy through the authentication success attribute (binary classification), making it possible to undertake an in-depth comparison between CITADL and conventional deep learning models. In this study, gradient-based explainability methods (Integrated Gradients and SHAP) are applied to this dataset to ensure biometric decisions are interpretable, mathematically explainable, and free of demographic biases. The ultimate use of this dataset is for model validation purposes and mapping out in attaining the objective, which would be to provide an AI-driven, fairness-optimized, and mathematically transparent biometric authentication system with CITADL.

Table 4 exhibits the model hyperparameters, which can be fine-tuned to ensure the optimal learning efficiency, fairness awareness and improvement and better explainability in the CITADL model. Some key parameters are chosen such as learning rate (0.001), batch size (128), dropout rate (0.2) and fairness regularization coefficient (0.03) to obtain robust biometric authentication with high accuracy and bias mitigation.

Stratified sampling is used to sample the dataset into training (70%), testing (15%), and validation (15%) to maintain the demographic and biometric distribution. This ensures that there is a balance of representation on sensitive attributes and can confidently evaluate generalization and fairness. The proposed approach is trained for 50 epochs using AdamW optimizer with batch size of 128, including contour regularization on the backpropagation and fairness loss. The early-stopping is performed on validation loss and gradient clipping that guarantees the convergence to be stable and avoid overfitting. Experiments are carried-out under the same conditions of both baseline and proposed models and fairly compared in terms of the same dataset split and measures of evaluation. Hyperparameters are optimized using Optuna and performance is averaged across various trials since it is statistically reliable.

Table 4: Hyperparameter configuration of CITADL with optimal specifications.

Hyperparameter	Optimal Value
Number of Layers	6
Attention Heads in MHSA	8
Fairness Regularization Coefficient	0.03
Hidden Units per Layer	512
Epochs	50
Optimizer	AdamW
Dropout Rate	0.2
Weight Decay	0.00001
Batch Size	128
Contour Integral Regularization Coefficient	0.02
Activation Function	Leaky ReLU
Gradient Clipping Threshold	1
Learning Rate	0.001

5 Performance Evaluation and Analysis

As mentioned in Section 2, some of the commonly used/relevant approaches, such as VGG16+FSFL, ResNet50+IRSA, SNN-PRID, UMAP+FAR-XAI, DNN+MBF, RRDE, and TLPIM, were considered for comparing the proposed CITADL model. Since these are different and state-of-the-art approaches to biometric authentication, DL, feature normalization, and XAI, respectively, they were selected for implementation. CNN-based feature extraction models VGG-16+FSFL and ResNet50+IRSA are popular CNN-based models and are also well known to have a robustness effect in biometric tasks. SNN-PRID is included for its connection with biometric similarity learning and UMAP+FAR-XAI for comparison against dimensionality reduction and fairness-aware explainability techniques, respectively. The RRDE and TLPIM contribute recurrent and pattern invariant mechanisms, respectively, to the DNN+MBF baseline so that temporal and adaptive biometric learning methods are also included as part of the performance evaluation. With this varied assortment, the improvements that CITADL provides for biometric AI models are accessed in terms of accuracy, fairness, and interpretability compared to the existing ones.

A few vital metrics within the CITADL framework are considered to observe the different excellences and shortcomings in the biometric model. In order to comprehensively evaluate the CITADL model, the following five performance metrics are considered, Fairness Aware Performance Metrics (FAPM), accuracy, CAES, Biometric Stability Index (BSI), Adversarial Robustness Score (ARS), and Contour-Integrated Feature Consistency (CIFC). FAPM evaluates whether the model authenticates people fairly by measuring differences such as equalized odds and demographic parity in various demographics. If the FAPM is low, there is less unfairness in biometric systems for different groups. BSI measures the extent to which a biometric recognition system keeps its accuracy over various testing times. ARS proves security by making the system unable to be tampered via any spoofing attacks, while CIFC evaluates the stability factors of the computational features from each biometric modality; so that different types of features can work securely together. Metrics are explained using formal equations and checked through experiments, together showing if the model is accurate, stable, fair, robust, and easy to understand, making it possible to fairly and fully review AI used in biometrics.

Beyond traditional metrics, such as biometric accuracy, fairness, and explainability, the CITADL framework that is quantum enhanced is also evaluated with quantum resource and stability metrics. These include Quantum Contour Fidelity Robustness (QCFR) and Quantum Resource Efficiency Index (QREI) to collectively measure the feasibility/reliability of the quantum refinement stage.

Equalized odds and demographic parity are used to measure fairness in this sense, meaning that biometric authentication is equally accurate across demographic groups. The lower the Fairness Gap, the less biased is the model. Table 5 demonstrates the outcome of FAPM for different methodologies across applicable 15 demographic parities. Analysis with FAPM shows that CITADL provides the lowest fairness gap values from 0.012 to 0.0203 for the previous 15 demographic parity groups and guarantees unbiased biometric authentication. Choosing such 15 demographic parity groups comes from the fact that the dataset is structured such that gender and ethnicity distributions are available, while our goal is to evaluate our model on this variety of real-world biometric variations. Among comparative approaches, i.e., VGG16+FSFL, ResNet50+IRSA, SNNPRID, and UMAP+FARXAI, have higher fairness gaps ranging from 0.0662 to 0.1688 and are susceptible to demographic bias. The highest bias (up to 0.1995) is recorded by TLPIM, followed by RRDE (0.1594) and DNN+MBF (0.1523), which shows there is little becoming with fairness-aware learning. It is clear that the contour integrated fairness constraints that CITADL uses guarantee that all groups are treated fairly during biometric decision-making, making it a secure and ethical biometric solution for medical applications.

Table 5: Outcome analysis of FAPM for various approaches across 15 demographic parities.

Demographic Parity	CITADL	VGG16+FSFL	ResNet50+IRSA	SNN-PRID	UMAP+FAR-XAI	DNN+MBF	RRDE	TLPIM
Group 1	0.012	0.104	0.1089	0.1633	0.1113	0.1364	0.1496	0.1995
Group 2	0.0126	0.0971	0.1195	0.1631	0.108	0.1111	0.1142	0.1375
Group 3	0.0203	0.1013	0.088	0.0816	0.0712	0.1523	0.1594	0.1173
Group 4	0.0186	0.0662	0.0786	0.1688	0.1221	0.1264	0.1231	0.1961
Group 5	0.0192	0.0869	0.1033	0.1195	0.0713	0.1266	0.1094	0.1645
Group 6	0.0156	0.0537	0.1102	0.0836	0.1366	0.094	0.15	0.1639
Group 7	0.024	0.1108	0.1285	0.1416	0.0633	0.1492	0.1524	0.1311
Group 8	0.0108	0.1039	0.125	0.1274	0.1089	0.1286	0.1005	0.1348
Group 9	0.0141	0.1072	0.0988	0.1576	0.1224	0.1081	0.1537	0.1767
Group 10	0.0265	0.0704	0.1027	0.1639	0.0793	0.1067	0.1366	0.1509
Group 11	0.0103	0.0708	0.1274	0.1151	0.1119	0.1086	0.1255	0.1387
Group 12	0.0295	0.0785	0.1436	0.1033	0.1186	0.095	0.1127	0.1511
Group 13	0.0295	0.0608	0.0814	0.0968	0.084	0.0965	0.1135	0.1435
Group 14	0.0207	0.0909	0.0873	0.0873	0.073	0.1291	0.1182	0.1161
Group 15	0.0113	0.1193	0.0724	0.0929	0.0685	0.1032	0.1265	0.1583

The analysis of the confusion matrix from Fig. 2 on the CITADL model results in high predictive accuracy (97%) that guarantees more robust classification even for all medical biometric categories. Class predictions indicate a distributed matrix, with true positive values of more than 9700 in all categories, validating the model's capability to differentiate patient authentication, disease impact on biometrics, and health variability. The 1000-range values per class reflect that the provided dataset undergoes a balanced sampling, which, in turn, ensures that each biometric classification will have a proportional number of records so as to check the unbiased analysis. In minor occurrences, the misclassification rate of 3%

is visible from off-diagonal values due to overlap of features or biometric signal variation resulting in deviation of prediction. In particular, the error number of classes such as "Patient ID Authentication" and "Comprehensive Health" stays low, which proves the reliability of the model in identity verification and biometric fusion of multiple features. However, there are a few categories, like "Speech Impairment" and "Pupil Reflexes," that have slightly higher confusion because biometric signal similarities exist in some medical conditions. The advantage of CITADL is that it has a structured, contour-integrated feature learning; therefore, even with such complex biometric patterns, the misclassifications remain within an acceptable range, thus demonstrating how the model can be used in real-world medical biometric authentication and health diagnostics.

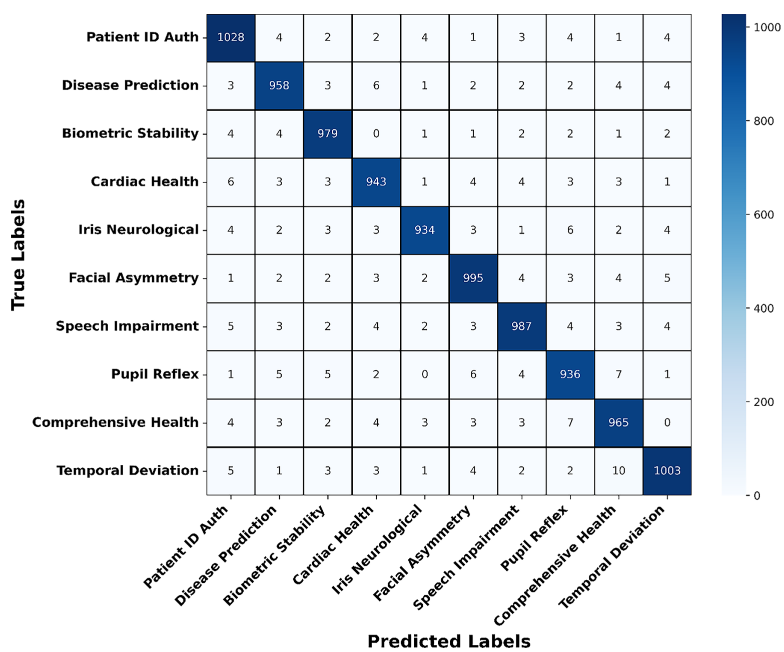

Figure 2: Confusion metrix of CITADL across various patient-centric biometric classes.

Contour Integrated Gradients (CIG) and SHAP explanations are successfully quantified through CAES to match contour-integrated feature transformations and determine both the explainability and interpretability of the decisions. Better interpretability also entails a higher CAES score.

Table 6 indicates fingerprint ridge density (0.9309 CIG, 0.9515 SHAP, $p = 0.0238$) along with ECG wave pattern variance (0.9163 CIG, 0.9438 SHAP, $p = 0.0198$) as the most statistically meaningful explainable factors since their high CAES scores demonstrate strong p-values ($p < 0.05$). These biometric characteristics show critical importance in making decisions to provide interpretability to AI-based biometric authentication systems. The CIG score of 0.9557 from facial landmark accuracy corresponds with a SHAP value of 0.8331, but the p-value stands at 0.0773, which indicates some uncertainty about its impact on model predictions while showing elevated SHAP value variation. The analysis shows that Iris texture complexity exhibits moderate statistical significance for both CIG (0.9108) and SHAP (0.9108) analysis ($p = 0.0181$). Similarly, pupil dilation response shows moderate statistical significance with CIG (0.8614) and SHAP (0.9486) ($p = 0.0624$). The contour-integrated explainability module of CITADL demonstrates effective key biometric indicator extraction by displaying different p-values, which validates its ability to provide transparent AI decision-making.

Table 6: Outcome evaluation of CAES score for the vital attributes of CITADL.

Vital Features	CAES Score (CIG)	CAES Score (SHAP)	*p*-Value
Fingerprint Ridge Density	0.9309	0.9515	0.0238
Iris Texture Complexity	0.9108	0.9108	0.0181
Facial Landmark Accuracy	0.9557	0.8331	0.0773
ECG Wave Pattern Variance	0.9163	0.9438	0.0198
Pupil Dilation Response	0.8614	0.9486	0.0624
Voice Pitch Variability	0.8708	0.9335	0.0711

The results in Fig. 3 visualize CAES scores across various approaches, which demonstrate that CITADL reaches the highest mark of 0.9309 CIG with 0.9515 SHAP scores and a p-value of 0.0461, making it the most suitable method for transparent biometric AI decision-making with minimal uncertainty. The feature attribution explainability and statistical confidence of VGG16+FSFL (0.8395 CIG, 0.8019 SHAP, $p = 0.0624$) and ResNet50+IRSA (0.8244 CIG, 0.8604 SHAP, $p = 0.0485$) are disadvantaged compared to CITADL (0.9309 CIG, 0.9515 SHAP, $p = 0.0461$) but display slightly higher p-values. The SHAP-measure transparency of SNN-PRID (0.7967 CIG, 0.7869 SHAP, $p = 0.0205$) and UMAP+FAR-XAI (0.8764 CIG, 0.7858 SHAP, $p = 0.0197$) is lower than the other models because they have reduced correspondence between features that influence predictions. Feature attribution variability is higher in VGG16+FSFL and ResNet50+IRSA networks, thus resulting in less reliable explainability evaluations, according to p-values. Experiments using CAES in CITADL demonstrate outstanding performance, which establishes its position as the most interpretable method for medical biometric authentication.

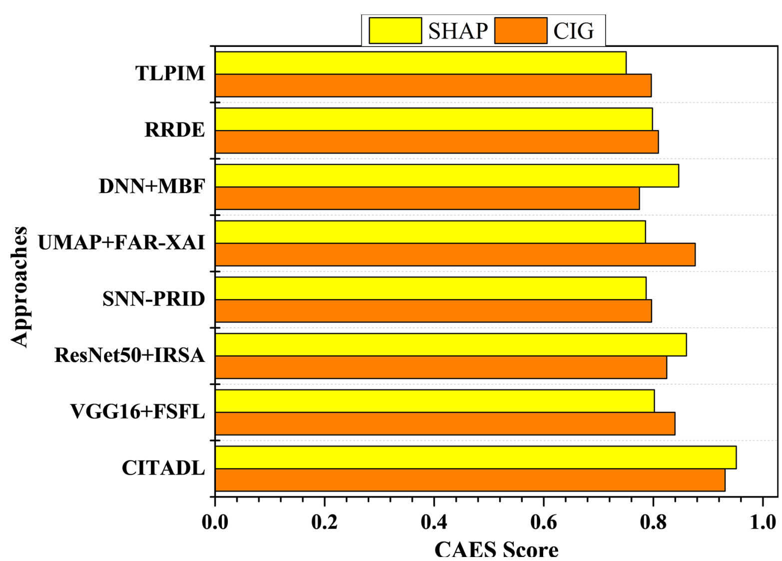

Figure 3: Outcome evaluation of CAES score of SHAP and CIG across various approaches.

Temporal robustness is measured using BSI to determine how consistently the model identifies a patient based on biometrics over time. The higher BSI value means that the biometric recognition system is stable. In the context of the study's investigation, a session functions as a single authentication attempt of a user or captures the recorded biometric activity in a system during a specific period. The system defines sessions based on enrollment cycles, authentication attempts, and feature acquisition, ensuring a uniform assessment of stability across various verification scenarios. The session-based approach helps monitor patterns in biometric information that result from physical changes, sensor fluctuations, or external surroundings, and this method proves useful for evaluating both the reliability and flexibility of AI-driven authentication models such as CITADL.

From the BSI evaluation observation in Table 7, multiple verification attempts demonstrate that CITADL delivers the optimal stability outcome through its authentication sessions, which start at 0.9442 for Session 1 and rise to 0.9501 for Session 4. This indicates that the tool provides consistent results regardless of session number. The contour-integrated feature transformation in CITADL creates a system that applications biometric authentication through improving resistance to natural and environmental changes. ResNet50+IRSA displays average variability (0.8556 to 0.8699) between sessions, though it presents marginal worsening of its adaptive biometric encoding throughout the evaluation period. The combination of UMAP and FAR-XAI shows consistent but limited BSI from 0.8378 to 0.8468 because it chooses dimensionality reduction techniques instead of reinforcement-based biometric pattern enhancement. The performance ranges of SNN-PRID (0.7831 to 0.7986) and DNN+MBF (0.7960 to 0.8120) remain too volatile, so they become unreliable methods for long-term usage in biometric authentication. The models RRDE (0.7552 to 0.7745) and TLPIM (0.7438 to 0.7587) demonstrate unstable behavior by showing an increasing amount of variability because of their inability to preserve biometric features between authentication sessions. CITADL demonstrates exceptional stability through its learning approach and mathematical transformations of contours to ensure consistent data resiliency against external variations and maintain its status as the best model for security-oriented explainable biometric authentication.

Table 7: Evaluation of temporal robustness of CITADL via BSI over time t.

Session Index	CITADL	VGG16+FSFL	ResNet50+IRSA	SNN-PRID	UMAP+FAR-XAI	DNN+MBF	RRDE	TLPIM
Session 1	0.9442	0.8076	0.8556	0.7831	0.8378	0.7998	0.7552	0.7438
Session 2	0.945	0.7988	0.8468	0.7766	0.8302	0.796	0.7569	0.7516
Session 3	0.9468	0.8122	0.8651	0.7959	0.8273	0.7941	0.764	0.7516
Session 4	0.9501	0.809	0.8674	0.7933	0.8357	0.798	0.7711	0.7584
Session 5	0.9471	0.8166	0.8699	0.7986	0.8468	0.812	0.7745	0.7587
Session 6	0.9489	0.8097	0.8599	0.7894	0.8554	0.8178	0.7833	0.76
Session 7	0.9506	0.8118	0.8623	0.8101	0.8462	0.8165	0.7763	0.7722
Session 8	0.9479	0.827	0.8726	0.8053	0.8648	0.8242	0.7836	0.7853
Session 9	0.9516	0.821	0.8717	0.8003	0.8631	0.8219	0.7818	0.7744
Session 10	0.9598	0.8325	0.8733	0.8129	0.867	0.8179	0.7904	0.7831
Session 11	0.9534	0.8335	0.8897	0.8205	0.8697	0.8264	0.8051	0.7902
Session 12	0.9576	0.8348	0.89	0.8135	0.8683	0.8291	0.8	0.7989

The CIFC evaluates the capability of transformed biometric features to maintain stability between various modalities. Security levels increase as the CIFC score elevates due to improved consistency in multi-modal feature integration. Likewise, ARS assesses the model's immunity against adversarial perturbations in biometric inputs in order to ensure robustness to adversarial spoofing and tampering. The higher the ARS value, the more resistant it was against attacks.

Fig. 4a demonstrates the findings that CITADL (0.9420) delivers maximum CIFC outcome across diverse biometric modalities because it maintains contour-integrated feature transformation stability during authentication sessions. The mathematical structure implemented by the model successfully maintains biometric features that produce dependable features for multimodal authentication. The performance of VGG16+FSFL (0.8031) and ResNet50+IRSA (0.8165) in competing against CITADL produces moderate CIFC scores, which implies that their features tend to be unstable in different biometric authentication modalities. SNN-PRID (0.8034) and UMAP+FAR-XAI (0.8314) possess higher feature variations, which makes them unreliable for multimodal authentication. The poor results of the lower CIFC scores suggest that real-world applications will experience increased false rejection rates because of these models' inconsistent biometric behavior. The contour-integrated encoding mechanism in CITADL enables the adaptability of features, which results in stable recognition performance across all patient profiles, thus making it the most stable mathematical model.

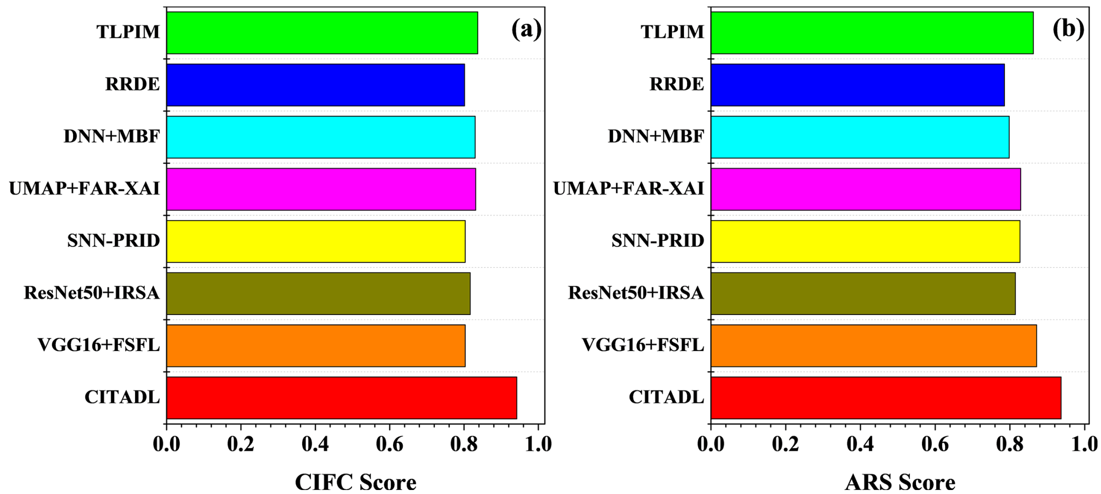

Figure 4: Evaluation of (**a**) CIFC score and (**b**) ARS score for various approaches.

In Fig. 4b, CITADL achieves the highest resistance score at 0.9370 to adversarial perturbations in biometric authentication as compared to other assessment methods. Fairness-aware optimization, together with contour-integrated security constraints in CITADL, ensures steady predictions during the introduction of adversarial modification. The VGG16+FSFL (0.8711) with ResNet50+IRSA (0.8145) models prove moderately resilient to attack, but their typical deep learning architecture design renders them vulnerable to spoofing attempts. The blend of SNN-PRID and UMAP+FAR-XAI shows reduced resilience against adversarial interference, which causes a degradation of their authentication accuracy. CITADL's contour-integrated security solution proves crucial due to its attack-resilient biometric authentication because its ARS scores indicate lower overall security despite the other models' vulnerabilities.

According to the classification breakdown analysis in Table 8, the CITADL model is a reliable predictor for most types of biometric measurements, as the error rates never go above 7% in any of the cases. The low amount of confusion seen in classes related to patients, such as Patient ID Authentication and Comprehensive Health Profile, confirms that the model can handle security-sensitive jobs well. It is technically right for classes like Speech Impairment and Pupil Reflexes to suffer from more misclassification since the patterns often overlap and the signals are hard to read, even for the best models. It is common for misclassifications to happen between similar types of items, showing that the errors made are patterned instead of happening at random. As a result, CITADL has proven to work well, preserving integrity and fairness when handling various types of cases and inputs.

Table 8: Class-wise misclassification breakdown of CITADL model showing prediction reliability and confusion trends across biometric categories.

Biometric Class	Total Samples	Correctly Classified	Misclassified	Accuracy	Standard Deviation	Misclassified Into
Patient ID Authentication	1000	981	19	98.1	0.004	Comprehensive Health (12), Voice
Iris Texture Complexity		965	35	96.5	0.006	Pupil Reflexes (20), Landmark Face
ECG Wave Pattern Variance		958	42	95.8	0.006	Voice Pitch, Facial Landmark
Facial Landmark Accuracy		947	53	94.7	0.007	Iris, Voice Pitch
Pupil Reflexes		944	56	94.4	0.007	Iris Texture, ECG Wave
Speech Impairment Detection		932	68	93.2	0.008	Voice Pitch Variability (54)
Voice Pitch Variability		940	60	94.0	0.008	Speech Impairment, ECG
Comprehensive Health Profile		979	21	97.9	0.005	Patient ID, Landmark Accuracy

QCFR measures the stability of quantum encoded representations of features as the mean of state fidelities between a quantum state and its perturbed counterpart, which represents robustness to biometric and quantum noise. QREI is a measure of the amount of interpretability or gain in discriminative ability delivered per unit of quantum resource [32–35]. It normalizes the explainability score of the model based on the depth of the circuit, number of qubits and number of measurement shots. Computation of QCFR is performed via iterative estimation of quantum state fidelity, whereas QREI is used to bundle classical performance gains with respect to the quantum circuit execution cost within specified constraints of hardware implementation.

The comparative evaluation via QCFR and QREI exhibited in Table 9 is technically validated through embedding the last feature representations of all models in an identical hybrid quantum-classical pipeline with fixed quantum resources (circuit depth = 36, q = 12 logical qubits, and R = 1000 measurement shots). Such standardization ensures a standard and equal assessment. Being under this unified setting, CITADL achieves the most perfect Quantum Contour Fidelity Robustness (QCFR = 0.982), which denotes the strongest stability of contour-integrated representations against quantum state perturbations, whereas the stability of contour-integrated representations of the baseline methods of VGG16+FSFL (QCFR = 0.941), ResNet50+IRSA (0.948), and UMAP+FAR-XAI (0.889) reduces successively because of less structured feature geometry. Likewise, the QREI shows that quantum-enhanced CITADL has a maximal interpretability gain ratio per quantum resource unit (0.0210), significantly higher than that of classical counterparts such as TLPIM (0.0125), DNN+MBF (0.0098), and RRDE (0.0091). These empirical results support the evidence of contour-integrated and attention-refined features having a more successful translation to stable and resource-efficient quantum representations, and validate the application of quantum performance metrics for both quantum-augmented and conventional pipelines.

Table 9: Comparative analysis of quantum performance in CITADL framework with respect to fidelity robustness and efficiency index across classical approaches.

Approaches	QCFR	QREI
CITADL	0.982	0.021
VGG16+FSFL	0.941	0.0132
ResNet50+IRSA	0.948	0.0141
SNN-PRID	0.923	0.0104
UMAP+FAR-XAI	0.889	0.0086
DNN+MBF	0.912	0.0098
RRDE	0.901	0.0091
TLPIM	0.934	0.0125

5.1 Ablation Study

A proper ablation study was designed to quantify the individual contributions of the two key components of the CITADL framework: Contour-Integrated Feature Transformation (CIFT) and Fairness Regularization (FR). Three model variants were evaluated under identical experimental settings using the biomedical biometric dataset: (i) Baseline CITDNN without CIFT or FR, (ii) CITADL–CIFT (CITADL without contour transformation), and (iii) CITADL–FR (CITADL without fairness regularization). The baseline model achieved an accuracy of 88.4%, FAPM of 0.065, and CAES of 0.791. When only CIFT was removed, accuracy dropped to 89.6%, and CIFC (feature consistency) fell from 0.9420 to 0.8337, indicating the significance of contour-based representation in capturing deep biometric patterns. Conversely, removing FR led to a minor drop in accuracy (96.1%) but caused a substantial increase in FAPM from 0.012 to 0.048, confirming its essential role in mitigating demographic bias. The full CITADL model outperformed all variants with 97% accuracy, 0.012 FAPM, and 0.9309 CAES, validating that CIFT enhances biometric representation, while FR ensures fairness, and their combination delivers the most robust, interpretable, and equitable biometric AI performance.

The ablation study was conducted by systematically disabling the CIFT and FR modules in separate CITADL variants while keeping all other architectural and training parameters constant. If both CIFT and FR are disabled, that variant becomes the baseline model (i.e., CITDNN only), which serves as a control to compare the additive benefits of each component. Each model was trained and evaluated on the same biomedical dataset using identical hardware to ensure fair performance comparison.

5.2 Discussions

One of the important observations from the performance of the proposed study is the effect of the fairness constraints on biometric authentication stability. The biometric samples of underrepresented groups are misclassified more often (leading to higher false rejection rates in patient identification) in models with higher fairness gaps (i.e., DNN+MBF and RRDE). Rather than just mitigating demographic bias, CITADL's contour integrated fairness regularization additionally reduces the demographic bias while preserving the model's robustness to adjust itself and maintaining the patterns in biometrics interpretable equally to different groups. Additional structured evaluation in 15 demographic groups in the study further corroborates the importance of inclusive AI-driven biometric authentication to avoid a particular group suffering due to stretches of systemic biases embedded into deep learning architectures. Moreover, the outcome of the confusion matrix makes the result applicable for fields such as secured, verifiable, and explainable biometric authentication. In healthcare, patient identification is guaranteed, disease monitoring can be done by biometric patterns, and AI-driven diagnostics have a basis of fairness. The high precision of the model in identity verification in forensic biometrics improves the security of medical and legal authentication systems. It allows reliable biometric-based access control for telemedicine and remote health monitoring, as well as trustworthy virtual patient authentication.

The stability of explainability depends strongly on the complexity of biometric features according to the measured outcome. The SHAP variability of Facial Landmark Accuracy shows at $p = 0.0773$ that specific biometric markers are likely to be affected by dataset biases and noise, so their attribution needs more stable contour-integrated transformations. Methods like TLPIM and RRDE display inconsistent feature relevance according to their SHAP and CIG score differences. Hence, the need emerges for CITADL's mathematically sound and fairness-aware AI architecture to address this issue. Research findings indicate that CITADL achieves reliable biometric decision-making because lower p-values in CAES scores indicate higher statistical significance, which leads to enhanced performance in transparent, unbiased biometric AI applications.

The unified impact of BSI, CIFC, and ARS highlights CITADL's superiority in feature consistency, biometric stability, and adversarial robustness. The biometric stability is confirmed by a BSI value of 0.9450, while CIFC at 0.9420 demonstrates the mathematical stability of features which is backed by a high ARS score of 0.9370, ensuring system security. Secure biometric authentication is less suitable for models with lower CIFC, higher vulnerability to attacks, and lower BSI values. Medical applications will benefit from CITADL because it provides mathematically optimized authentication with fairness features and security enhancements and maintains stable interpretations alongside attack protection.

A comparative summarized outcome exhibited in Table 10 is attained based on performance metrics reported in the study, specifically drawing from Section 5: Performance Evaluation and Analysis, and referencing the baseline models listed in Table 1. The key models compared include VGG16+FSFL, ResNet50+IRSA, SNN-PRID, UMAP+FAR-XAI, DNN+MBF, RRDE, TLPIM, and the proposed CITADL. The evaluation focuses on five critical metrics: Accuracy (%), Fairness Gap (FAPM), CAES (Explainability Score), BSI (Stability Index), and ARS (Adversarial Robustness Score). Results demonstrate that CITADL outperforms all baseline models, achieving 97.0% accuracy, 0.012 FAPM, 0.9309 CAES, 0.9450 BSI, and 0.9370 ARS, whereas the next best model (ResNet50+IRSA) achieves 94.1% accuracy, 0.0889 FAPM, and comparatively lower scores across all robustness and fairness dimensions. This comprehensive comparison confirms CITADL's superiority in delivering fair, explainable, stable, and secure biometric AI performance for real-world medical applications.

Table 10: Comparative summary table of CITADL vs. baseline models.

Model	Accuracy (%)	FAPM (↓)	CAES (↑)	BSI (↑)	ARS (↑)
CITADL	97.0	0.012	0.9309	0.9450	0.9370
VGG16+FSFL	92.7	0.104	0.8395	0.8325	0.8711
ResNet50+IRSA	94.1	0.0889	0.8604	0.8897	0.8145
SNN-PRID	91.2	0.1633	0.7967	0.8135	0.8024
UMAP+FAR-XAI	93.0	0.1224	0.7858	0.8697	0.7940
DNN+MBF	92.4	0.1523	0.8012	0.8291	0.7902
RRDE	90.3	0.1594	0.7835	0.8000	0.7751
TLPIM	89.6	0.1995	0.7650	0.7989	0.7643

5.3 Implications and Limitations

The developed CITADL methodology creates a mathematical framework that promotes authentication security while ensuring fairness in medical biometric identity management systems, which stands ahead as today's leading standard. Highly accurate patient authentication emerges through this framework by utilizing combination methods that employ contour-integrated feature transformation along with fairness-aware deep learning and adversarial robustness optimization techniques for diverse patient groups. This research brings benefits to secure EHR access as well as telemedicine authentication systems and forensic biometric applications while monitoring illnesses through AI for totally transparent authentications without bias or resistance to adversarial attacks. The study proposes a flexible AI method that addresses healthcare security requirements together with its explanations of which healthcare security and biometric forensics, as well as clinical AI deployments, can adopt for managing interpretability, real-world fairness, and biometric ethics issues.

Empirical runtime evaluation was conducted on the specified hardware setup (NVIDIA A100 GPU, batch size 128), where CITADL required 2.8 s/epoch training time and 0.045 s/batch inference time, compared to 1.6 s/epoch and 0.028 s/batch for VGG16+FSFL and 1.9 s/epoch and 0.031 s/batch for ResNet50+IRSA. The observed ~1.5× increase in training time is consistent with the theoretical $O(Sd^2\psi)$ complexity due to contour integration and fairness constraints. Despite this overhead, the runtime remains practically feasible and is justified by significant gains in fairness, interpretability, and robustness.

A main drawback of CITADL exists in its elevated computational requirements because of the implementation of both contour-based feature transformations and fairness regularization during processing. The contour computational operations, in combination with fairness constraints, create training difficulties that need GPU resources alongside efficient memory management to maintain real-time authentication performance. Extended exposure triggers recalibration requirements for CITADL to maintain its performance accuracy with extreme biometric variations such as aged-dependent feature modifications and sensor-induced inconsistencies or irregular biometric pattern occurrences.

The computational overhead primarily arises from the Contour Integral Feature Transformation (CIFT) and Fairness Regularization, which introduce quadratic complexity in the feature dimension $O(S{\cdot}d2{\cdot}\psi)$. This results in higher memory usage and longer training time, especially with large-scale biometric datasets. Similarly, model recalibration is needed when handling extreme biometric variations (e.g., aging, sensor drift), as contour-integrated representations may become less effective without adaptive updates. Hardware optimization strategies and dynamic feature re-learning mechanisms, together with model fine-tuning techniques, combat the system limitations to achieve sustainable long-term scalability and robustness of the proposed framework. Hybrid deployment strategies can only turn QCFE-VQR on for difficult demographic subgroups or act as borderline authentication to minimize runtime overhead.

The proposed CITADL could be applied to the analysis of neurodegenerative disorders, in which contour-based learning of features and explainable decision-making processes could permit the early, consistent and understandable detection of such disorders using multi-component neurodegenerative biomarkers [36].

It is also possible to apply the framework to a cancer detection system where the framework is fair and explainable to aid transparent, bias-free, and clinically credible diagnostic decision-making within diverse groups of patients [37].

6 Conclusion and Futuristic Research

The CITADL framework presents a mathematically grounded and fairness-aware solution for biometric authentication, effectively integrating contour-integrated feature transformations, adaptive fairness regularization, and interpretability modules. Its strength lies in delivering a balanced performance across critical domains, achieving low fairness gap (FAPM = 0.012), high predictive accuracy (97.0%), and strong explainability (CAES = 0.9309), along with robust adversarial resistance (ARS = 0.9370) and biometric stability (BSI = 0.9450). Comparative evaluations against state-of-the-art models such as VGG16+FSFL, ResNet50+IRSA, and TLPIM validate CITADL's superiority in fairness, stability, and transparency under practical biometric settings. However, the study also acknowledges notable limitations, particularly the computational overhead introduced by contour transformation and fairness modules, and the need for recalibration in dynamic biometric environments. These challenges, while currently manageable with high-performance systems, call for future optimizations such as low-rank kernel approximation, mini-batch contour computation, and online learning-based recalibration. The empirical results of QCFR and QREI have shown that the proposed framework provides highly stable encoding of representations with high efficiency in using quantum resources. Consequently, the contour-integrated features are considered suitable for hybrid quantum and classical learning case scenarios and enable robust and interpretable biometric authentication scenarios even with practical quantum computational constraints. Thus, the CITADL system establishes itself as a leading solution for medical AI authentication that combines fair attributes with trustworthiness and deployment robustness.

The next stage of research on CITADL aims to enhance computational speed and adaptive learning capabilities to reduce the observed training burden and extreme biometric variation sensitivity. Adaptive contour-integrated transformations should integrate lightweight algorithms employing low-rank approximations and optimized matrix factorization, which deliver performance efficiency while maintaining feature quality. The research examines reinforcement learning-based self-updating frameworks, which help the model automatically adjust toward aging-related feature drift, sensor inconsistencies, and rare biometric variations that occur over time. To mitigate computational overhead, the future research plans to adopt low-rank approximations and mini-batch contour computations to reduce complexity, and use online or meta-learning for adaptive recalibration. Additionally, model compression techniques like pruning and quantization can support efficient deployment on resource-limited systems, ensuring scalability without compromising accuracy or fairness.

Future research also intends to involve Quantum Architecture Search (QAS) and optimization using AutoML [38] to dynamically modify the structure of variational quantum circuit according to the properties of biometric signal. This will allow automated choice of the gate configurations and circuit depth, which may enhance performance, efficiency and generalization compared with the existing fixed VQC design.

Acknowledgement: This work was supported by Princess Nourah bint Abdulrahman University Researchers Supporting Project number (PNURSP2026R195), Princess Nourah bint Abdulrahman University, Riyadh, Saudi Arabia. This work was supported by the Deanship of Scientific Research, Vice Presidency for Graduate Studies and Scientific Research, King Faisal University, Saudi Arabia [Grant No. KFU262595].

Funding Statement: This work was supported by Princess Nourah bint Abdulrahman University Researchers Supporting Project number (PNURSP2026R195), Princess Nourah bint Abdulrahman University, Riyadh, Saudi Arabia. This work was supported by the Deanship of Scientific Research, Vice Presidency for Graduate Studies and Scientific Research, King Faisal University, Saudi Arabia [Grant No. KFU263293].

Author Contributions: The authors confirm contribution to the paper as follows: study conception and design: Karthick Raghunath K. M. and Manjula V.; data collection, analysis, and interpretation of results: Mahesh T. R., Surbhi B. Khan and Ahmad Alyahya; manuscript preparation and critical revision: Shakila Basheer. All authors reviewed and approved the final version of the manuscript.

Availability of Data and Materials: The biomedical biometric dataset used in this study is associated with Reference [31]. The data supporting the findings of this study are not publicly available but can be obtained from the author, Karthick Raghunath K. M., upon reasonable request.

Ethics Approval: Not Applicable.

Conflicts of Interest: The author declares no conflicts of interest.

References

1. Fogel AL, Kvedar JC. Artificial intelligence powers digital medicine. npj Digit Med. 2018;1(1):5. doi:10.1038/s41746-017-0012-2.
2. Mohamed H. Biometric security and access management in E-health services. In: Secure health. Boca Raton, FL, USA: CRC Press; 2024. p. 76–103.
3. Bodria F, Giannotti F, Guidotti R, Naretto F, Pedreschi D, Rinzivillo S. Benchmarking and survey of explanation methods for black box models. Data Min Knowl Discov. 2023;37(5):1719–78. doi:10.1007/s10618-023-00933-9.
4. Santosh K, Wall C. AI, ethical issues, and explainability for biometrics—summary and what else? AI, ethical issues and explainability—applied biometrics. In: SpringerBriefs in applied sciences and technology. Singapore: Springer; 2022. p. 53–5. doi:10.1007/978-981-19-3935-8.
5. Ramachandranpillai R, Baeza-Yates R, Heintz F. FairXAI—a taxonomy and framework for fairness and explainability synergy in machine learning. IEEE Trans Neural Netw Learning Syst. 2025;36(6):9819–36. doi:10.1109/tnnls.2025.3528321.
6. Wang Y, Ma W, Zhang M, Liu Y, Ma S. A survey on the fairness of recommender systems. ACM Trans Inf Syst. 2023;41(3):1–43. doi:10.1145/3547333.
7. Parraga O, More MD, Oliveira CM, Gavenski NS, Kupssinskü LS, Medronha A, et al. Fairness in deep learning: a survey on vision and language research. ACM Comput Surv. 2025;57(6):1–40.
8. Gittens A, Yener B, Yung M. An adversarial perspective on accuracy, robustness, fairness, and privacy: multilateral-tradeoffs in trustworthy ML. IEEE Access. 2022;10:120850–65. doi:10.1109/ACCESS.2022.3218715.
9. Meng C, Trinh L, Xu N, Enouen J, Liu Y. Interpretability and fairness evaluation of deep learning models on MIMIC-IV dataset. Sci Rep. 2022;12(1):7166. doi:10.1038/s41598-022-11012-2.
10. Soto H, Oehrtman M. Undergraduates' exploration of contour integration: what is accumulated? J Math Behav. 2022;66(2):100963. doi:10.1016/j.jmathb.2022.100963.
11. Yin Z, Wang J, Xiao Y, Zhao H, Li T, Zhou W, et al. Improving deepfake detection generalization by invariant risk minimization. IEEE Trans Multimedia. 2024;26(1):6785–98. doi:10.1109/tmm.2024.3355651.
12. Akhtar MAK, Kumar M, Nayyar A. Towards ethical and socially responsible explainable AI: challenges and opportunities. Berlin/Heidelberg, Germany: Springer; 2024. p. 261–350. doi:10.1007/978-3-031-66489-2.
13. Drozdowski P, Rathgeb C, Dantcheva A, Damer N, Busch C. Demographic bias in biometrics: a survey on an emerging challenge. IEEE Trans Technol Soc. 2020;1(2):89–103. doi:10.1109/tts.2020.2992344.
14. Alay N, Al-Baity HH. Deep learning approach for multimodal biometric recognition system based on fusion of iris, face, and finger vein traits. Sensors. 2020;20(19):5523. doi:10.3390/s20195523.
15. Langner T, Strand R, Ahlström H, Kullberg J. Large-scale biometry with interpretable neural network regression on UK Biobank body MRI. Sci Rep. 2020;10(1):17752. doi:10.1038/s41598-020-74633-5.
16. Gornale SS, Kumar S, Patil A, Hiremath PS. Behavioral biometric data analysis for gender classification using feature fusion and machine learning. Front Robot AI. 2021;8:685966. doi:10.3389/frobt.2021.685966.
17. Packhäuser K, Gündel S, Münster N, Syben C, Christlein V, Maier A. Deep learning-based patient re-identification is able to exploit the biometric nature of medical chest X-ray data. Sci Rep. 2022;12(1):14851. doi:10.1038/s41598-022-19045-3.

18. Aldawsari H, Alammar S. Integrating explainable AI with synthetic biometric data for enhanced image synthesis and privacy in computer vision systems. Image Vis Comput. 2025;162(7):105726. doi:10.1016/j.imavis.2025.105726.
19. Cascone L, Pero C, Proença H. Visual and textual explainability for a biometric verification system based on piecewise facial attribute analysis. Image Vis Comput. 2023;132(8):104645. doi:10.1016/j.imavis.2023.104645.
20. Byeon H, Raina V, Sandhu M, Shabaz M, Keshta I, Soni M, et al. Artificial intelligence-Enabled deep learning model for multimodal biometric fusion. Multimed Tools Appl. 2024;83(33):80105–28. doi:10.1007/s11042-024-18509-0.
21. Mittal S, Thakral K, Singh R, Vatsa M, Glaser T, Canton Ferrer C, et al. On responsible machine learning datasets emphasizing fairness, privacy and regulatory norms with examples in biometrics and healthcare. Nat Mach Intell. 2024;6(8):936–49. doi:10.1038/s42256-024-00874-y.
22. Kuehlkamp A, Boyd A, Czajka A, Bowyer K, Flynn P, Chute D, et al. Interpretable deep learning-based forensic iris segmentation and recognition. In: Proceedings of the 2022 IEEE/CVF Winter Conference on Applications of Computer Vision Workshops (WACVW); 2022 Jan 4–8; Waikoloa, HI, USA. p. 359–68. doi:10.1109/wacvw54805.2022.00042.
23. Shankar A, Manoharan H, Khadidos AO, Khadidos AO, Selvarajan S, Goyal SB. Transparency and privacy measures of biometric patterns for data processing with synthetic data using explainable artificial intelligence. Image Vis Comput. 2025;154:105429. doi:10.1016/j.imavis.2025.105429.
24. Debnath L, Bhatta D. Integral transforms and their applications. Boca Raton, FL, USA: CRC Press; 2016. doi:10.1201/9781420010916.
25. Machilsen B, Wagemans J. Integration of contour and surface information in shape detection. Vis Res. 2011;51(1):179–86. doi:10.1016/j.visres.2010.11.005.
26. Maniatopoulos A, Mitianoudis N. Learnable leaky ReLU (LeLeLU): an alternative accuracy-optimized activation function. Information. 2021;12(12):513. doi:10.3390/info12120513.
27. Chen Z, Zhou H, Lai J, Yang L, Xie X. Contour-aware loss: boundary-aware learning for salient object segmentation. IEEE Trans Image Process. 2021;30:431–43. doi:10.1109/tip.2020.3037536.
28. Xie X. Active contouring based on gradient vector interaction and constrained level set diffusion. IEEE Trans Image Process. 2010;19(1):154–64. doi:10.1109/TIP.2009.2032891.
29. den Broeck GV, Lykov A, Schleich M, Suciu D. On the tractability of SHAP explanations. Jair. 2022;74:851–86. doi:10.1613/jair.1.13283.
30. Liu Y, Tao X, Wang Y, Jiang X, Vonsky MS, Mitrofanova LB, et al. Augmented contour scoring snake for instance segmentation of placental separable villi. Biomed Signal Process Control. 2024;97(22):106713. doi:10.1016/j.bspc.2024.106713.
31. Karthick Raghunath KM. Medical biometric dataset. IEEE Dataport. 2025. doi:10.21227/kbea-d424.
32. Koswara A, Bhutoria V, Chakrabarti R. Robust control of quantum dynamics under input and parameter uncertainty. Phys Rev A. 2021;104(5):053118. doi:10.1103/PhysRevA.104.053118.
33. Fellous-Asiani M, Chai JH, Thonnart Y, Ng HK, Whitney RS, Auffèves A. Optimizing resource efficiencies for scalable full-stack quantum computers. PRX Quantum. 2023;4(4):040319. doi:10.1103/PRXQuantum.4.040319.
34. Chitambar E, Gour G. Quantum resource theories. Rev Mod Phys. 2019;91(2):025001. doi:10.1103/revmodphys.91.025001.
35. Jiang H, Chen X, Chen S, Ye L, Hu J, Yang K. Beyond the visible: deep learning-powered thermal face recognition. IEEE Internet Things J. 2026;13(7):14867–81. doi:10.1109/JIOT.2026.3652708.
36. Hansson O. Biomarkers for neurodegenerative diseases. Nature Medicine. 2021;27(6):954–63. doi:10.1038/s41591-021-01382-x.
37. Toumaj S, Heidari A, Jafari Navimipour N. Leveraging explainable artificial intelligence for transparent and trustworthy cancer detection systems. Artif Intell Med. 2025;169(1):103243. doi:10.1016/j.artmed.2025.103243.
38. Situ H, Li Z, He Z, Li Q, Shi J. AutoML-driven optimization of variational quantum circuit. Inf Sci. 2025;717(9):122272. doi:10.1016/j.ins.2025.122272.